Beyond diffusion-limited aggregation kinetics in microparticle suspensions

Randall M. Erb,[1,*] Melissa D. Krebs,[2] Eben Alsberg,[2] Bappaditya Samanta,[3] Vincent M. Rotello,[3] and Benjamin B. Yellen[1]
[1]*Mechanical Engineering and Materials Science, Center for Biologically Inspired Materials and Material Systems, Duke University, Durham, North Carolina 27708, USA*
[2]*Department of Biomedical Engineering, Case Western Reserve University, Cleveland, Ohio 44106, USA*
[3]*Department of Chemistry, University of Massachusetts, Amherst, Massachusetts 01003, USA*
(Received 3 May 2009; revised manuscript received 15 August 2009; published 2 November 2009)

Aggregation in nondiffusion limited colloidal particle suspensions follows a temporal power-law dependence that is consistent with classical diffusion limited cluster aggregation models; however, the dynamic scaling exponents observed in these systems are not adequately described by diffusion limited cluster aggregation models, which expect these scaling exponents to be constant over all experimental conditions. We show here that the dynamic scaling exponents for 10 μm particles increase with the particle concentration and the particle-particle free energy of interaction. We provide a semiquantitative explanation for the scaling behavior in terms of the long-ranged particle-particle interaction potential.

DOI: 10.1103/PhysRevE.80.051402 PACS number(s): 82.70.Kj, 47.65.Cb, 61.43.Hv, 87.18.Ed

I. INTRODUCTION

Aggregation of colloidal particle suspensions under externally applied magnetic and electric field has been studied for decades both to gain new insight into nucleation processes occurring in a variety of colloidal systems [1–3] as well as the technical applications in vibration control [4,5], rotor sealant [6], flow control in microsystems [7], and more recently in the formation of linear cellular structures for potential tissue engineering applications [8]. For systems of colloidal particles smaller than a few microns, it is well accepted that the prevailing diffusion limited cluster aggregation (DLCA) theory can adequately explain experimental observations. However, the theory has been less successful for large colloidal systems, which are not strongly affected by thermal fluctuations and experience larger particle-particle interactions.

Numerous theoretical and experimental investigations have been conducted to study the dynamics of field-driven chain growth in colloidal particle suspensions. For particles, which experience strong magnetic interactions, the aggregation process is considered to be irreversible—in effect the aggregation process occurs by random diffusion, undergoing permanent binding when two diffusing species make physical contact [9,10]. Vicsek and Family uncovered a universal property in the DLCA model in two dimensional (2D) computer experiments, where they discovered that the aggregation process was characterized by constant dynamic scaling exponents [11,12], independent of the particle concentration or particle-particle interaction strength. These findings were confirmed both in computer models and experimentally by several authors for particles up to a few microns in size [2,13–15].

However, for particles on the order of 10 μm, recent reports have indicated that the dynamic scaling exponent can strongly depend on the particle-particle interaction strength, and moreover, can exhibit in some cases smaller dynamic scaling exponents ($z<1/3$) than predicted to be possible by the DLCA theory [2,8]. The goal of this article is to investigate the kinetics of chain growth in systems of 10 μm colloids immersed in a concentrated suspension of $\sim$10 nm iron oxide nanoparticles known as ferrofluid. Nonmagnetic colloids suspended in ferrofluid behave as magnetic holes and offer many experimental benefits over traditional paramagnetic colloidal systems. First, it is easier to tune the magnetic interaction between nonmagnetic particles both by changing the external field strength and the ferrofluid concentration [2]. Second, these systems allow for the utilization of the "image force" to repel particles away from the ferrofluid/glass surface, and thus allow for analysis of aggregation kinetics in bulk fluid with reduced interference by local surface inhomogeneities and interfacial forces [16–19].

In this work, we extend previous experimental analysis of chain growth in large colloidal particle suspensions, and include for the first time the role in nonmagnetic particle concentration on the dynamic scaling exponents. We offer a qualitative explanation for the inconsistency between DLCA models and the results presented here, by illustrating the long-ranged nature of the dimensionless interaction potential between 10-μm sized particles. The rest of this manuscript is organized as follows. In Sec. II, we review the basic principles of negative magnetophoresis. In Sec. III, we review dynamic scaling theory for colloidal systems and outline its role in field-driven aggregation of nonmagnetic colloids in ferrofluid. Materials and methods are described in Sec. IV, followed by the presentation of experimental results in Sec. V. The relevance of these results compared with other works is discussed in Sec. VI, followed by a brief conclusion in Sec. VII.

II. NEGATIVE MAGNETOPHORESIS

When large inclusions such as nonmagnetic microparticles are introduced into the ferrofluid, they will behave like point dipoles when subjected to an external uniform magnetic field. According to classical magnetostatic field theory,

*Mailing address: Duke University, 144 Hudson Hall, Durham, NC, 27708, USA. FAX: (919)-660-8963; randall.erb@duke.edu

the effective dipole moment of the particle is given by:

$$\vec{m}_n = 3\frac{\mu_n - \mu_f}{\mu_n + 2\mu_f} V_n \vec{H}, \tag{1}$$

where V_n is the volume of the microparticle, $\mu_n \approx \mu_0$ and μ_f are the magnetic permeabilities of the microparticle and ferrofluid, respectively, where μ_0 is the magnetic permeability of free space. The magnetic permeability of the ferrofluid can be adjusted by controlling the concentration of magnetic nanoparticles in the ferrofluid. For low-ferrofluid concentrations, the magnetic susceptibility of ferrofluid is linearly proportional to the volume fraction of magnetic nanoparticles in the fluid, ϕ_f, and the magnetic permeability is:

$$\mu_f = \mu_o[1 + \phi_f \vec{M}_S L(\xi)/\vec{H}]. \tag{2}$$

The Langevin function, $L(\xi) = \coth \xi - 1/\xi$, is confined to range between 0 and 1 with the argument $\xi(H) = \mu_o M_s V_f |\vec{H}|/k_B T$ representing the dimensionless particle-particle interaction strength compared to randomizing thermal fluctuation energy. Here, $\vec{M}_s$ refers to the saturation magnetization of the nanoparticle material, while V_f denotes the volume of a typical magnetic nanoparticle in the ferrofluid. The ferrofluid employed in these experiments is similar to the magnetic nanoparticle suspensions used in a previous work [3], which had a magnetic susceptibility that was linearly dependent on the volume fraction of magnetic nanoparticles ϕ_f. Furthermore, the magnetic diameter of these particles was found to be approximately 12 nm compared to its core diameter of 10.3 nm, indicating the absence of field-induced aggregation in these ferrofluids. Finally, the fields employed in this work have been kept relatively weak (100 Oe), for which the magnetic energy of an individual nanoparticle is weaker than thermal energy, $\xi < 1$. This restriction allowed for the magnetic permeability of the ferrofluid to be approximated by the initial magnetic susceptibility of the magnetic nanoparticles $\chi = \mu_0 M_s^2 V/3k_B T$ and the volume concentration ϕ_f, as $\mu_f = \mu_0(1 + \chi\phi_f)$

Nonmagnetic colloidal particles inside ferrofluid attract one another and form chains through dipole-dipole interactions. The free energy of magnetostatic interaction between two particles depends on the type of fields used both to magnetize the particles and apply the field gradient, (see Appendix for more details). A dimensionless parameter, $\lambda = A_{\max}/k_B T$, is typically used to characterize the magnitude of the dipole-dipole interactions within these suspensions, where $A_{\max}$ is the free energy of interaction between two touching particles whose moments are aligned collinear to the position vector between the particle centers, expressed as

$$A_{\max} = \frac{3}{4}\mu_o V_n \left(\frac{\mu_n - \mu_f}{\mu_n + 2\mu_f}\right)^2 \vec{H}_{ext}^2. \tag{3}$$

According to Eqs. (2) and (3), the particle-particle interaction energy can be altered not only by modulating the applied field, but also by changing the ferrofluid concentration, as done in this work. In fact, changing the ferrofluid concentration as opposed to the external field strength is a better method for adjusting the interaction energy because the magnetic susceptibility of the ferrofluid follows a linear relationship with the ferrofluid concentration, as opposed to a nonlinear constitutive relationship with the external field.

Finally, a key reason why ferrofluids are ideal for these dynamical studies is because they allow for chain growth experiments to be conducted with reduced interference by the fluid boundaries through utilization of repulsive "image forces" at the ferrofluid/glass interface. The interested reader is referred to several papers to learn more about the topic of image forces [16–19]. When the image force is strong enough, the particle is observed to levitate above the fluid/glass interface to a position where the image force exactly cancels gravitational and other surface forces in the system. In many cases, the image force can be so strong that it levitates the particle by a diameter or more away from the substrate and nearly completely eliminates the effect of surface forces. By exploiting this image repulsion phenomenon, we are able to study chain growth in a quasi-2D system, thus allowing for direct comparison with the 2D computer simulations performed by others [11].

III. DYNAMIC SCALING THEORY

By convention, the state of growth of particle chains is quantified using the parameter $S(t)$ and $L(t)$, which represents the weighted aggregate size, defined as:

$$S(t) = \frac{\sum_s n_s(t)s^2}{\sum_s n_s(t)s}, \quad L(t) = \frac{\sum_s n_s(t)s}{\sum_s n_s(t)}, \tag{4}$$

where s is the number of particles in a given chain, and n_s is the number density of chains of length s. Dynamic scaling theory predicts that the rate of chain growth should follow a power law as $S(t) \sim t^z$, where z is a dynamic scaling exponent. In the work of Vicsek and Family [11], many of these power-law dependences have been proposed and experimentally demonstrated to conform to the following scaling relationship,

$$n_s(t) \sim t^{-w} s^{-\tau} f(s/t^z). \tag{5}$$

The function $f(s/t^z)$ approaches 1 when $s \ll t^z$ and approaches 0 for $s \gg t^z$. This function characterizes the effect of smaller clusters being incorporated into larger clusters. The exponent w represents another dynamic scaling exponent that describes the reduction of $n_s(t)$ with time for each aggregate size, s. The static exponent, τ, describes the general relation between cluster sizes and cluster densities that is consistent throughout many systems including the theory of thermal and geometrical critical points [20,21].

An alternative form to Eq. (5) brings to light the crossover exponent, Δ, which is written as

$$n_s(t) \cdot s^2 \sim (s/t^z)^{\Delta}, \tag{6}$$

where it follows that $\Delta = w/z$. Monitoring the crossover exponent allows observation of distinct regimes of the aggregation process. The two possible regimes for the aggregation process include

$$\Delta = \begin{cases} 2-\tau & for \quad \mathcal{LL} \quad aggregation \\ 2 & for \quad \mathcal{LS} \quad aggregation \end{cases}, \tag{7}$$

where $\mathcal{LL}$ aggregation refers to systems that predominantly undergo aggregation of all cluster sizes simultaneously, while $\mathcal{LS}$ aggregation refers to systems wherein the inclusion of smaller clusters (in the limit, single particles) into larger clusters is the predominant mechanism for the aggregation process.

Based on these relationships, DLCA models have been developed to describe the aggregation of particle systems whose capture kinetics are dominated by thermal diffusion. Aggregation processes driven by isotropic diffusion have been observed to exhibit a dynamic scaling exponent of $z \approx 1.4$, which is independent of the initial particle concentration [3]. Processes driven by anisotropic diffusion, such as growth of colloidal particle chains in an applied magnetic or electric field, are observed in experiments and computer simulations to display a different dynamic scaling exponent of $z \approx 0.5$, due to the reduced probability of two clusters making physical contact except under certain constrained orientations [22]. The two regimes of aggregation kinetics described above represent the limits of very weak and strong particle interactions, respectively. Regardless, in past experiments and numerical simulations for smaller particles, the dynamic scaling exponent was found to be constant and independent of the particle-particle interaction strength or the initial particle concentration [2,13]. On the other hand, large particles, which are not strongly influenced by Brownian motion have been observed to display scaling exponents that are dependent both on the interaction potential, λ, and have magnitudes that are outside of the generally expected range for smaller particles [2,8]. Thus, the main motivation for this work was to further investigate these reported inconsistencies, and in particular determine how the dynamic scaling exponents depend on the particle-particle interaction energy and particle concentration using an experimental apparatus, which removes the effect of surface forces on the aggregation kinetics.

IV. MATERIALS AND METHODS

To test the particle aggregation dynamics, 10 μm polystyrene particles with a polydispersity of $<3\%$ (Duke Scientific, Palo Alto, CA) were used. The ferrofluid consisted of iron oxide nanoparticles stabilized by a surface coating of Bovine Serum Albumin (BSA), and were synthesized according to the authors' previously reported methods [23]. The ferrofluid concentration used in our experiments ranged from 0.28% to 0.7% by volume and were previously tested for biocompatibility allowing applicability of our findings to certain biological systems [8]. This concentration range corresponds to a respective zero-field susceptibility range of $\mu_f = 1.06\mu_o$ to $\mu_f = 1.15\mu_o$, according to Eq. (2). The saturation magnetization of the ferrofluid was assumed to be $M_S = 0.6T/\mu_o$ [A/m], consistent with previous saturation measurements for 12 nm iron oxide ferrofluids [24]. In order to allow the particles sufficient room to be repelled via image forces, fluid cells were constructed by using 120 μm spacers (Invitrogen, Eugene, OR) to separate a coverslip and a microscope slide, in which a suspension of ferrofluid and microparticles was inserted and hermetically sealed.

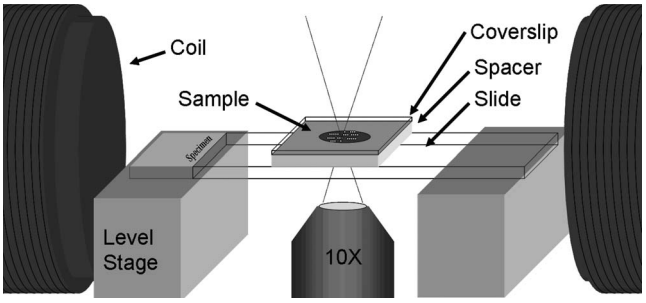

FIG. 1. The experimental setup consists of two solenoids and a level sample stage used to view the chain growth experiments via inverted fluorescent microscopy through a 10X objective. A suspension of microparticles and ferrofluid is filled into a fluid spacer and pressed between a microscope slide and cover slip.

For 10 μm particles, gravitational forces sediment the particles on short time scales, thus the fluid cells were observed via inverted reflected light microscopy, as shown in Fig. 1. The sample was placed upon a highly leveled, vibration isolation table to avoid translational particle drift which tends to increase aggregation rates. In order to minimize particle-surface forces, cleaned microscope slides were first rinsed thoroughly with ethanol to produce hydrophobic surfaces. The microscope slides were then incubated in 5 mg/mL solution of Bovine Serum Albimum (Sigma Aldrich, St. Louis, MO) in 1X Phosphate Buffer Saline (Teknova, Holister, CA). This treatment was found to prevent the strong adhesive forces between the particle and surface and allow for the particle to be released from the surface via image forces upon application of the external field. The ferrofluid's optical attenuation of the particles' fluorescence allowed us to evaluate when the particles repelled from surface. When the surface treatment protocol described above was used, $>99\%$ of the particles were repelled from the substrate.

Magnetic fields were applied in-plane with the glass slides using solenoids containing iron cores, shown in Fig. 1. The field variation over the sample was $<1\%$, as measured with a gaussmeter (Lakeshore, Westerville, OH). Chain growth was studied by video microscopy using a 10X objective that allowed for a field of view containing a large number of particles, $N \gg 500$. The kinetics of chain growth was studied using a digital camera (QImaging Retiga 2000R) that compiled still images every 30 s for a minimum of 1800 s. Automated image analysis was found to produce inaccurate and variable results due to large intensity differences over time, and thus, the images were analyzed manually, counting aggregate sizes by hand.

V. EXPERIMENTAL RESULTS

A typical time sequence for the nonmagnetic particles exposed to uniform 100 Oe external field is presented in Figs. 2(a)–2(d). As time progresses, the effective cluster size increases dramatically, producing long chains of nonmagnetic

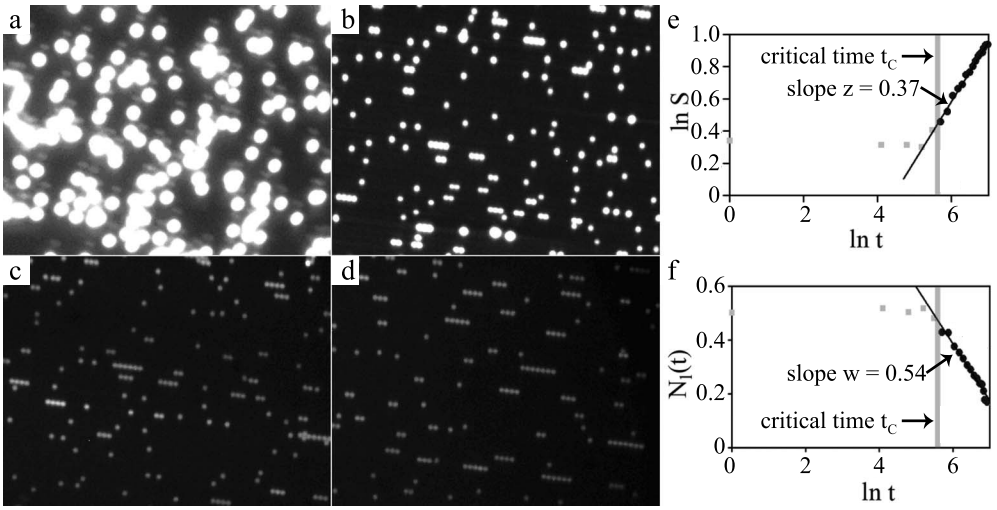

FIG. 2. Time sequence of micrographs for ϕ_n=2.4% and ϕ_f=0.4% showing growth of particle chains at various times: a) 0 s, b) 300 s, c) 600 s, and d) 1600 s. Particle intensity decreases due to image forces repelling particles from interface. Temporal evolution of both e) the effective cluster length and f) the number of single particles is shown. The best fitting slopes of the data after particles reached equilibrium height, (gray line), represent dynamic exponents of z and w, respectively.

particles in ferrofluid, and the fluorescence intensity decreases from the image force repelling the particles into the ferrofluid. In our initial experiments with untreated glass slides, the interfacial forces (i.e., DLVO, depletion, and electrostatic forces) were found to be extremely important and prevented the particles from lifting off the substrate due to image force. Presumably, the Van der Waals interaction was so strong that the particles were unable to escape out of the secondary energy minimum that was located nanometers from the surface even in the strongest magnetic field, often appearing to stick on localized surface defects. On the other hand, when the surfaces were passivated with a BSA monolayer the nonspecific surface interactions were dramatically reduced and the particles were observed to move away from the substrate due to the image force, as is clearly evident in Figs. 2(c) and 2(d).

Figure 2(e) shows a log-log plot of the scaling parameter, S, as a function of time. The initial data points, as $t \to 0$, exhibit near-zero slope due to the characteristic time required for an initial aggregation event of two clusters at average initial separation to come together [12]. To reduce the influence of surface effects in data interpretation, data was analyzed only after the particles reached the quasi-2D plane where a force balance between gravitational and image force was obtained. This critical time point, t_c, was experimentally determined when the particles' average intensity became static. For $t > t_c$, the slope exhibits a power law dependence over many temporal data points. The dynamic exponent w can also be attained by plotting the time progression of $n_s(t)$ for a given aggregate size, (e.g., $s=1$ for individual particles), as shown in Fig. 2(f). For all experiments, the evolution of $n_s(t)$ for $t > t_c$ follows a strict power-law dependence of $n_s(t) \sim t^{-w}$.

In this work, we systematically tested the dependence of the scaling exponents, z and w, on both the nonmagnetic particle concentration and the ferrofluid concentration. The results of all experimental trials are presented in Fig. 3 and Table I. Clearly, z and w are not constant over all experimental conditions, contrary to predictions by DLCA models, and this deviation is conceivably attributed to the strong particle-particle interactions that dominate Brownian diffusion in this experimental system. Figures 3(a) and 3(b) represents the dynamic exponents w and z as functions of the nonmagnetic particle concentration in a fixed 100 Oe external field while the magnetic particle concentration is kept constant. Both w and z increase in roughly linear fashion with increasing nonmagnetic particle concentrations. Figures 3(c) and 3(d) dis-

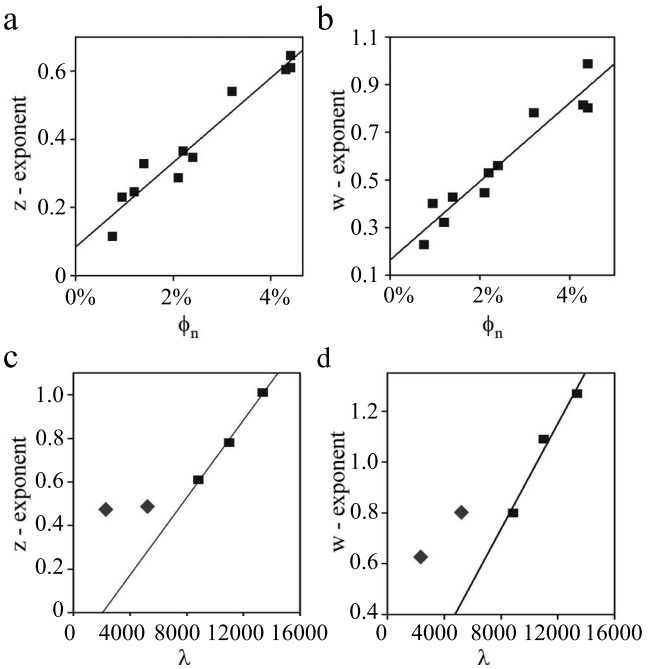

FIG. 3. Dynamic exponents of (a, c) z and (b, d) w versus ϕ_n and λ, respectively, including non surface-affected data points (squares) with straight lines for visual guidance, and surface-affected data points (diamonds).

TABLE I. The dynamic exponents of z, w, and Δ obtained for different experiments are displayed. Varied concentrations of the nonmagnetic and magnetic particles, ϕ_n and ϕ_f, respectively, are reported along with the nonmagnetic particle diameter, d, and calculated energy ratio, λ, for each experiment.

d (μm)	Φ_n	Φ_f	λ	z	z'	w	Δ
10	0.75%	0.56%	8840	0.12	0.09	0.23	1.97
10	0.95%	0.56%	8840	0.23	0.16	0.40	1.75
10	1.20%	0.56%	8840	0.25	0.17	0.32	1.31
10	1.40%	0.56%	8840	0.33	0.22	0.43	1.30
10	2.10%	0.56%	8840	0.29	0.26	0.45	1.55
10	2.20%	0.56%	8840	0.37	0.24	0.53	1.47
10	2.40%	0.56%	8840	0.35	0.26	0.56	1.61
10	3.20%	0.56%	8840	0.54	0.44	0.78	1.45
10	4.30%	0.56%	8840	0.60	0.45	0.82	1.35
10	4.40%	0.56%	8840	0.61	0.58	0.80	1.32
10	4.40%	0.56%	8840	0.65	0.44	0.99	1.53
10	3.40%	0.28%	2370	0.47	0.31	0.62	1.32
10	3.90%	0.42%	5146	0.49	0.38	0.80	1.63
10	4.40%	0.56%	8840	0.61	0.58	0.80	1.32
10	4.97%	0.63%	11000	0.78	0.59	1.09	1.40
10	4.80%	0.70%	13354	1.01	0.72	1.27	1.26

plays the measured values of the dynamic exponents w and z as the ferrofluid concentration is increased while maintaining a constant 100 Oe external field and constant nonmagnetic particle concentration.

VI. DISCUSSION

This work presents the first empirical evidence that the relationship between ϕ_n and the dynamic scaling exponents w and z is correlated as seen in Figs. 3(a) and 3(b). In addition, we observed that the relationship between λ and the dynamic scaling exponents was also correlated when ϕ_n was held constant. This correlation was only observed when $\lambda > 6000$, for which the image force was sufficient to levitate the particles far from the interface. In effect, surface forces were completely eliminated for all experimental trials except the ones with the lowest ferrofluid concentrations, $\phi_f = 0.28\%$ and $\phi_f = 0.42\%$. As can be seen in Figs. 3(c) and 3(d), including our surface-affected data into this relationship would move our data closer to previous reports of the linear λ-dependence of these dynamic exponents [2]. These correlations do not occur for smaller particle sizes where particle energies are on the order of thermal energy and chain formation is in the regime of DLCA systems [2,7].

We propose a qualitative explanation for the observed scaling relationships for the "capture radius" of particles in suspension. The capture radius refers to the maximum distance for which two particles experience interaction potentials that exceed thermal fluctuation energy, k_BT. An upper bound for the capture radius can be obtained from Eq. (3) using the assumption that the magnetic moments of two particles are aligned parallel to the position vector between the particle centers. This criterion allows for the calculation of the effective separation distance between two particles, $\delta_{\max}$, for which the interaction potential is equal to thermal fluctuations. The capture radius, $C.R.$, can be expressed as a dimensionless quantity in units of particle diameters, d, as

$$C.R. = \delta_{\max}/d_n = \sqrt[3]{A_{\max}/k_BT}. \tag{8}$$

This normalized capture radius scales linearly with the particle diameter, indicating that larger particles will have larger relative capture radii, and thus, are more likely to be influenced by potential energy interactions than by Brownian motion. In terms of realistic material parameters, the capture radius of 1 and 10 μm particles, while holding all other parameters fixed, ($\vec{H} = 100$ Oe, $\mu_f = 1.1\mu_o$, $\mu_n = \mu_o$), are calculated to be around 2 and 20 particle diameters, respectively. By comparison, we can consider the average separation distance between two particle positions to be a function of the particle's initial volume fraction, ϕ_n, assuming equally spaced hexagonal 2D packing, as $\delta/d = 0.78/\sqrt{\phi_n}$. This analysis shows why particles smaller than 1 micron are nearly always dominated by Brownian motion and, thus, conform to the DLCA model, since the average separation distance is always larger than the particle's capture radius, except at exceedingly high-particle concentration (nearly 7% volume fraction in this example). The 10-μm particles, on the other hand, are nearly always in the capture radius of nearby particles, except at exceedingly low-particle concentrations (around 0.07% vol. fraction in this example). Thus, the chain growth kinetics of 10 μm particles can be considered in the diffusion limited regime only at exceedingly low-particle concentrations.

The experimentally determined crossover exponent supports this argument through the observation of two different regimes in the aggregation kinetics. For example, at concentrations of nonmagnetic particles above 1% volume fraction, the crossover exponent remained constant across all trials at $\Delta = 1.43 \pm 0.12$ as shown in Fig. 4. This result indicates that systems in this regime, exhibiting crossover exponents $\Delta < 2$, are dominated by $\mathcal{LL}$ aggregation, as described in Eq. (7). Unlike many DLCA systems, the aggregation of these larger clusters is not limited by diffusion but by the kinetics of magnetic potential interactions, making the interactions between larger clusters more favorable than smaller clusters. However, at concentrations of nonmagnetic particles below 1% volume fraction, the crossover exponent appears to approach $\Delta = 2$, which is consistent with the $\mathcal{LS}$ aggregation regime. The predominant mechanism of aggregation in this regime is the inclusion of smaller clusters (e.g., single particles) into larger clusters and is evidence that diffusion may be playing a role in the most dilute experimental trials. This is not surprising as the more dilute suspensions have interparticle separations that are approaching the capture radius requirement for DLCA systems. An alternative method for double checking the crossover exponent is to plot $s^2 n_s(t)$ against $s/S(t)$, as reported by Meakin *et al.* [12], to elucidate the power-law dependence in Eq. (6). The crossover exponent calculated using both methods is shown in Fig. 4 to have nice agreement.

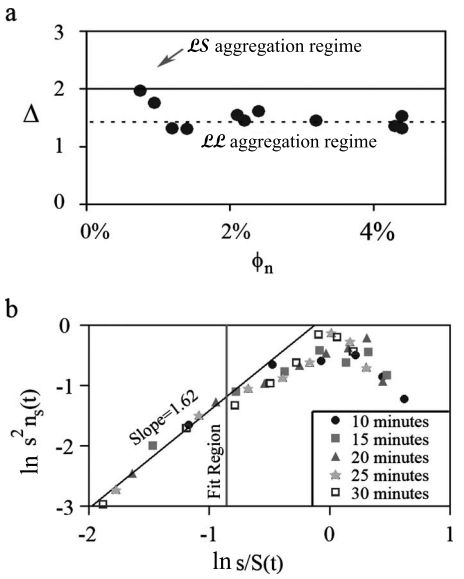

FIG. 4. Crossover dynamic exponents arrived at through a) calculating the ratio of w and z and b) the power law dependence detailed in Eq. (6) for $\phi_n=4.4\%$. Both methods demonstrate good agreement with crossover exponents of $\Delta<2$, indicating aggregation occurs between both small-large cluster groups, as well as large-large cluster groups.

VII. CONCLUSION

In this work, we present our investigations of the growth of 10 μm nonmagnetic particles inside ferrofluid in order to determine the kinetics of assembling non-Brownian particle suspensions. We discovered that the dynamic scaling exponents describing the kinetics of chain growth are dependent on the dimensionless particle-particle energy of interaction and on the particle concentrations of both the ferrofluid and the nonmagnetic particles. These results reveal that a new family of models is needed to accurately predict the scaling dynamics of nondiffusion limited particle aggregation systems.

ACKNOWLEDGMENTS

R.M.E. received support from the National Science Foundation (Grant No. DGE-0221632) and Medtronic. M.D.K. received support from the National Science Foundation. V.M.R. received support from the National Science Foundation (Grant No. CHE-0808945) and from the NIH (Grant No. GM077173).

APPENDIX

Following the convention of Landau and Lifshitz [25], we describe the interaction between two magnetizable particles in an external field at constant temperature in terms of the differential in the interaction free energy (32.4), given by

$$\delta A = -\vec{m}\cdot\delta\vec{H}_u, \tag{A.1}$$

where $\vec{m}$ is the magnetic moment of the first particle and $\vec{H}_u=\vec{H}_{ext}+\vec{H}_{dip}$ is the total field of the system in the absence of the first particle, including any external uniform fields, $\vec{H}_{ext}$, as well the dipolar field produced by the second particle, $\vec{H}_{dip}$. For convenience, here the magnetic moment is presented in units of Nm/Oe according to Eq. (1), and takes into account the permeability of the fluid, (see reference [26] for a detailed discussion on this topic).

The interaction free energy required to bring the first particle from infinitely far away into contact with the second particle is calculated by integrating the above expression; however some precautions must be taken during integration since there is not always a linear relationship between $\vec{m}$ and $\vec{H}_u$. In the case of no external uniform fields, the same field is responsible for magnetizing the particle and providing the field gradient for its attraction (i.e., $\vec{H}_u=\vec{H}_{dip}$ and $\vec{m}=\bar{\mu}V_n\vec{H}_{dip}$), thus, the interaction energy differential becomes

$$\begin{aligned}\delta A &\cong -\bar{\mu}V_n\vec{H}_{dip}\cdot\delta\vec{H}_{dip}\\ &= -\tfrac{1}{2}\bar{\mu}V_n\delta(\vec{H}_{dip}^2)\\ &= \delta\left(-\tfrac{1}{2}\vec{m}\cdot\vec{H}_{dip}\right)\\ \therefore A &= -\tfrac{1}{2}\vec{m}\cdot\vec{H}_{dip}.\end{aligned} \tag{A.2}$$

On the other hand, when a strong external field is applied, two different fields are responsible for the mechanical attraction between the two particles. In the case of weakly magnetic particle systems such as this one, the particle's magnetic moment is dominated by the spatially homogeneous external field and behaves as a constant with respect to integration. Likewise, the external uniform field has no differential (i.e., $\delta\vec{H}_u=\delta\vec{H}_{ext}+\delta\vec{H}_{dip}=\delta\vec{H}_{dip}$), thus, after integration the expression for interaction free energy becomes

$$A=\int\delta A=-\vec{m}\int\cdot\delta\vec{H}_u=-\vec{m}\cdot\vec{H}_{dip}, \tag{A.3}$$

which does not contain the $\frac{1}{2}$ term of Eq. (A.2). Unfortunately, this expression is not consistently used in the literature. For example, in references [2,13,26], this expression is used correctly, whereas in references [8,27,28] the $\frac{1}{2}$ term is incorrectly applied. For this reason, we use Eq. (A.3) for interaction free energy in this paper, given by:

$$A_{ij}=-\frac{\mu_o}{4\pi}\left[\frac{3(\vec{m}_i\cdot\hat{r}_{ij})(\vec{m}_j\cdot\hat{r}_{ij})-\vec{m}_i\cdot\vec{m}_j}{r_{ij}^3}\right]. \tag{A.4}$$

[1] S. L. Biswal and A. P. Gast, Phys. Rev. E **68**, 021402 (2003).
[2] J. Cernak, G. Helgesen, and A. T. Skjeltorp, Phys. Rev. E **70**, 031504 (2004).
[3] R. M. Erb *et al.*, Nature (London) **457**, 999 (2009).
[4] Z. P. Shulman *et al.*, J. Non-Newtonian Fluid Mech. **8**, 29 (1981).
[5] P. Dominguez-Garcia *et al.*, Phys. Rev. E **76**, 051403 (2007).
[6] T. A. Osman, G. S. Nada, and Z. S. Safar, Tribol. Int. **34**, 369 (2001).
[7] A. K. Vuppu *et al.*, J. Appl. Phys. **96**, 6831 (2004).
[8] M. D. Krebs *et al.*, Nano Lett. **9**, 1812 (2009).
[9] M. Kolb, R. Botet, and R. Jullien, Phys. Rev. Lett. **51**, 1123 (1983).
[10] P. Meakin and H. E. Stanley, Phys. Rev. Lett. **51**, 1457 (1983).
[11] T. Vicsek and F. Family, Phys. Rev. Lett. **52**, 1669 (1984).
[12] P. Meakin, T. Vicsek, and F. Family, Phys. Rev. B **31**, 564 (1985).
[13] J. H. E. Promislow and A. P. Gast, J. Chem. Phys. **102**, 5492 (1995).
[14] G. Helgesen *et al.*, Phys. Rev. Lett. **61**, 1736 (1988).
[15] D. Sohn, J. Magn. Magn. Mater. **173**, 305 (1997).
[16] R. M. Erb and B. B. Yellen, IEEE Trans. Magn. **42**, 3554 (2006).
[17] M. Warner and R. M. Horneich J. Phys. A **18**, 2325 (1985).
[18] R. Toussaint *et al.*, Phys. Rev. E **69**, 011407 (2004).
[19] A. T. Skjeltorp, Phys. Rev. Lett. **51**, 2306 (1983).
[20] D. Stauffer, Phys. Rep. **54**, 1 (1979).
[21] K. Binder, Ann. Phys. **98**, 390 (1976).
[22] S. Miyazima, P. Meakin, and F. Family, Phys. Rev. A **36**, 1421 (1987).
[23] B. Samanta *et al.*, J. Mater. Chem. **18**, 1204 (2008).
[24] M. F. Islam *et al.*, Phys. Rev. E **67**, 021402 (2003).
[25] L. D. Landau, L. P. Pitaevskii, and E. M. Lifshitz, *Electrodynamics of Continuous Media* (Elsevier Butterworth-Heinemann, Burlington, 2004).
[26] T. Jones, IEEE Trans. Ind. Appl. **IA-21**, 930 (1985).
[27] G. Helgesen, E. Svasand, and A. T. Skjeltorp, J. Phys.: Condens. Matter **20**, 204127 (2008).
[28] M. Hagenbuchle and J. Liu, Appl. Opt. **36**, 7664 (1997).